

APPLIED SCIENCES AND ENGINEERING

Lymphatic-draining nanoparticles deliver Bay K8644 payload to lymphatic vessels and enhance their pumping function

Lauren F. Sestito^{1,2}, Kim H. T. To³, Matthew T. Cribb^{3,4}, Paul A. Archer^{4,5}, Susan N. Thomas^{1,3,4,5*}, J. Brandon Dixon^{1,3,4*}

Dysfunction of collecting lymphatic vessel pumping is associated with an array of pathologies. S(-)-Bay K8644 (BayK), a small-molecule agonist of L-type calcium channels, improves vessel contractility *ex vivo* but has been left unexplored *in vivo* because of poor lymphatic access and risk of deleterious off-target effects. When formulated within lymph-draining nanoparticles (NPs), BayK acutely improved lymphatic vessel function, effects not seen from treatment with BayK in its free form. By preventing rapid drug access to the circulation, NP formulation also reduced BayK's dose-limiting side effects. When applied to a mouse model of lymphedema, treatment with BayK formulated in lymph-draining NPs, but not free BayK, improved pumping pressure generated by intact lymphatic vessels and tissue remodeling associated with the pathology. This work reveals the utility of a lymph-targeting NP platform to pharmacologically enhance lymphatic pumping *in vivo* and highlights a promising approach to treating lymphatic dysfunction.

INTRODUCTION

The lymphatic system is an often-overlooked component of the circulatory system that is critical in maintaining fluid balance in the body. Fluid that is lost from the blood by capillary filtration drains from the interstitium into lymphatic capillaries, and this fluid, termed lymph, is propelled back into circulation by a combination of the contraction of surrounding skeletal muscle (1) and artery pulsations (2) along with active contractions of the lymphatic vessels (LVs) themselves. Because lymphatic drainage is vital in transport and fluid balance, lymphatic dysfunction is associated with many pathologies. In the cardiovascular system, for example, the lymphatic system plays an important role in maintaining tissue health (3, 4). The lymphatic system is the primary route of reverse cholesterol transport responsible for amelioration of atherosclerosis (5, 6), lymphatic dysfunction often precedes atherosclerotic plaque formation (7), and alleviating lymphatic dysfunction can improve outcomes after myocardial infarction (8). Lymphatic dysfunction is also associated with diseases such as obesity (9, 10), diabetes (11), and lipedema (12). The most common lymphatic disease, however, is lymphedema, a complex pathology associated with both immune dysregulation and lymphatic dysfunction that occurs when lymphatic drainage is insufficient to maintain physiological interstitial fluid volumes (13). Secondary lymphedema, the more common manifestation of the disease, occurs because of post-natal insult to lymphatic vasculature such as radiation (14), surgical lymph node (LN) removal (15), or lymphatic filariasis infection (16). This lymphatic disruption causes impaired fluid flow and

clearance, resulting in fluid accumulation, tissue remodeling, altered immune cell infiltration, and inflammation (17–19). The contractility of LVs in patients with lymphedema is additionally impaired; lymphedematous legs show irregular contractions too weak to propel lymph (20), and lymphatic congestion lymphoscintigraphy measurements reveal lymphatic pump failure in patients with ipsilateral arm lymphedema after breast cancer surgery (21). These dysfunctions eventually result in lymphedema symptoms including edema, tissue remodeling and fibrosis, recurring infections, and pain.

Although lymphedema affects millions, the disease currently has no cure; patients are instead treated by compression and massage that can help manage symptoms of the disease but do not address the root inflammation or inadequate lymphatic drainage that promote lymphedema progression. While leukotriene B₄ antagonists such as ketoprofen (22) and bestatin (23) can reduce edema and pathologic tissue remodeling, their clinical success has been limited, and therapeutics are not currently part of a typical lymphedema treatment regimen. In addition, while it is well established that LV-pumping dysfunction is associated with lymphedema progression, amelioration of LV dysfunction remains an unexplored avenue for lymphedema treatment. There are also no existing therapeutics that can directly enhance lymphatic pumping *in vivo*, either clinically or in animal models.

LV-pumping function is regulated in part by L-type calcium channels on lymphatic muscle cells (LMCs) (24, 25) that have been targeted with small-molecule calcium channel agonists such as S(-)-Bay K8644 (BayK) *ex vivo* in the study of LV-pumping mechanisms (26–28). BayK, in particular, has been shown to improve functional metrics such as ejection fraction (27) and contraction amplitude (25) when applied to isolated rodent popliteal LVs. Although BayK is a promising regulator as it augments lymphatic contractility *ex vivo*, several barriers have stymied its *in vivo* application. First, small-molecule drugs such as BayK are challenging to deliver to lymphatic tissues. This is because although the

Copyright © 2023 The Authors, some rights reserved; exclusive licensee American Association for the Advancement of Science. No claim to original U.S. Government Works. Distributed under a Creative Commons Attribution NonCommercial License 4.0 (CC BY-NC).

¹Wallace H. Coulter School of Biomedical Engineering, Georgia Institute of Technology and Emory University, Atlanta, GA 30332, USA. ²Department of Mechanical Engineering and Bioengineering, Valparaiso University, 1900 Chapel Dr, Valparaiso, IN 46383, USA. ³George W. Woodruff School of Mechanical Engineering, Georgia Institute of Technology, Atlanta, GA 30332, USA. ⁴Parker H. Petit Institute for Bioengineering and Biosciences, Georgia Institute of Technology, Atlanta, GA 30332, USA. ⁵Winship Cancer Institute, Emory University, Atlanta, GA 30322, USA.

*Corresponding author. Email: susan.thomas@gatech.edu (S.N.T.); dixon@gatech.edu (J.B.D.)

most direct route into LVs is via drainage from the interstitium, small molecules injected in interstitial tissues are primarily absorbed into the bloodstream because of its large volume and high flow rates, resulting in rapid systemic exposure and poor lymphatic access (29, 30); the resulting low drug concentration within target LVs can thus limit drug efficacy or necessitate repeated or increased dosing. Because of the ubiquitous expression of L-type calcium channels on nontarget cells such as cardiac muscle cells (31), neurons (32), and skeletal muscle (33), systemic drug exposure also poses the risk of dangerous off-target effects (34). A major hurdle to the use of BayK, or other L-type calcium channel agonists, to treat lymphatic impairment is therefore the lack of appropriate drug delivery vehicles to optimize lymphatic uptake and access while minimizing systemic drug exposure and resulting side effects.

To overcome these limitations and enable the application of BayK for the treatment of lymphatic dysfunction *in vivo*, BayK was formulated into biocompatible nanoparticles (NPs) to enable its uptake into draining collecting LVs after injection in the skin. The NP vehicle used has an oily polymer core in which large amounts of hydrophobic small-molecule drug can partition without the need for drug modification or conjugation (35) and was formulated to a 30-nm diameter ideal for drainage into lymph of both the NP and its incorporated payload (30, 36). The size dependency of lymph drainage by locally administered nanomaterials has been well described (37), and particle platforms have been previously used by our group and others to improve drug uptake into the lymphatic system (35, 38, 39). However, all work to date that sought to improve therapeutic payload delivery to the lymphatic system focused on delivery to LNs and the cells they contain (immune cells, cancer cells, etc.) rather than the collecting LVs themselves. Whether enhancing the lymph abundance of a small-molecule drug could improve its direct *in vivo* effects on collecting LVs has yet to be established.

Using near-infrared (NIR) microscopy to image lymphatic pumping in real time, the *in vivo* effects of BayK on mouse tail collecting LVs were evaluated. A single administration of BayK increased LV-pumping function for 8 hours when formulated into lymph-draining NPs (BayK-NPs) but not in its free form. The NP formulation also reduced systemic BayK exposure and mitigated the side effects of administered free BayK. Daily administration of BayK-NPs, but not free BayK, rescued LV pumping pressure in a mouse tail model of secondary lymphedema (40), effects associated with reduced collagen deposition. Directing the effects of BayK within LVs thus represents a promising approach to improving LV-pumping function *in vivo* via intralymphatic delivery of small-molecule contractility enhancers and demonstrates that drug delivery technology can enable therapeutic modulation of LV pump function.

RESULTS

BayK is encapsulated in and gradually released from NP

Although L-type calcium channel agonist BayK is known to improve LV pumping *ex vivo* through its effects on LMCs (Fig. 1A), its *in vivo* effect on vessel function has not been explored because of its poor targetability resulting from its small size (356 Da). While small-molecule drugs such as BayK are unrestricted by extracellular matrix in the interstitium and can passively drain into both blood and lymph, they tend to partition primarily into

the blood due to its large volume and high flow rates (36, 37), resulting in poor lymphatic access. This effect is clearly observed in the mouse tail (Fig. 1B); when IRDye 680 is conjugated to 30-nm polypropylene sulfide (PPS) NP, it shows clear uptake into tail LVs, colocalizing with a known lymphatic-draining IRDye 800CW-labeled 20-kDa polyethylene glycol (PEG) tracer, although there is no overlap in the dye emissions (fig. S1A). When free IRDye 680 is injected, however, no visibly detectable signal is observed in LVs. An NP carrier can thus provide a clear lymphatic access advantage to the typical poor lymphatic uptake of a small molecule. To overcome this barrier to lymphatic delivery, BayK was encapsulated in NPs composed of a PPS core surface stabilized with Pluronic. Hydrophobic small-molecule drugs such as BayK partition within their hydrophobic PPS core upon mixing (Fig. 1C) (35, 41). To evaluate BayK encapsulation into these NP, elution of both BayK and NP from a size exclusion chromatography column was monitored before and after the components were mixed; BayK could be detected by its absorbance, which peaks at 415 nm (Fig. 1D) and can be used to generate a standard curve to determine BayK concentration (fig. S1B), and NP were detected using a modified iodine assay for the detection of the NP Pluronic (30). When BayK and NP were individually run on a size exclusion column, they showed distinct elution profiles, as expected on the basis of their size difference (Fig. 1E). When the two components were mixed, however, the BayK signal coeluted with the NP, suggesting successful encapsulation and the formation of BayK-loaded NPs (BayK-NPs) (Fig. 1F). Encapsulation of BayK did not affect NP size (Fig. 1G), which is critical for its lymphatic draining capabilities. BayK was released from BayK-NPs gradually *in vitro* over the course of days (Fig. 1H), with somewhat faster release at 37°C than at room temperature; 50% release occurred at ~8 and ~15 hours, respectively. Formulation within NP clearly improved BayK retention within the dialysis membrane, as free, unencapsulated BayK was completely lost within 8 hours. BayK could be encapsulated with high efficiency at tested conditions, with 90% of the drug loading into the NP core (Fig. 1I), and encapsulation could be tailored by adjusting the ratio of BayK:NP mixed (fig. S1C).

BayK-NPs enhance lymphatic pump function *ex vivo*

To directly evaluate the effect of BayK-NPs on LVs, rat mesenteric LVs were isolated and cannulated, their contractile response to BayK application *ex vivo* was monitored, and functional pumping metrics of contraction frequency, amplitude, and ejection fraction were calculated (Fig. 2, A to D). Free, unformulated BayK had immediate, dose-dependent effects on isolated vessel function upon addition to the bath, including increased pumping amplitude (Fig. 2B) and ejection fraction at as low as 200 nM BayK (Fig. 2C). Addition of free BayK to the bath similarly increased diastolic time, the time when the vessel was relaxed during diastole (fig. S2A), but contraction frequency (Fig. 2A) and fractional pump flow (fig. S2B) were unaffected by a free BayK dose up to 1000 nM. An immediate response was likewise observed in response to treatment with BayK-NP at a BayK dose of 200 nM that resulted in much less frequent but stronger contractions (Fig. 2E), consistent with the vessel response to free BayK at the same dose (Fig. 2D). Treatment with NP vehicle alone, in which no BayK was loaded, induced no discernable response by vessels (Fig. 2F); contraction frequency and amplitude remained consistent, indicating that the NPs, not to itself, have direct effects on vessel pumping. Overall, incubation

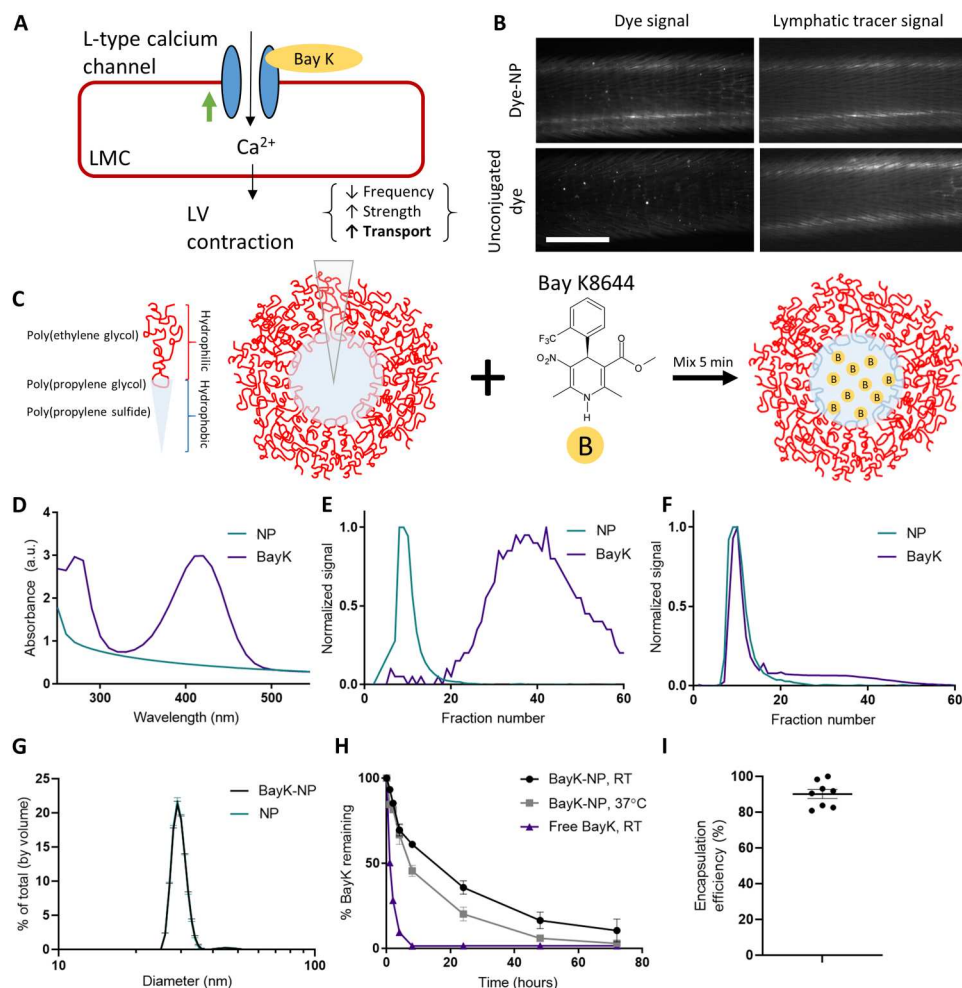


Fig. 1. NPs provide an LV-targeting advantage compared to free drug and allow for efficient loading and controlled release of small-molecule Bay K. (A) Schematic of BayK's effect on LV pumping. (B) Appearance of injected dye in tail collecting LVs (left) after coinjection with a lymphatic-draining PEG tracer (right). Scale bar, 3 mm. (C) Schematic of Pluronic-stabilized PPS NP structure and loading with hydrophobic small-molecule BayK. (D) Absorbance spectra of BayK and NPs. (E) Elution profiles of BayK and NP vehicle from a CL-6B size exclusion column when run separately or (F) after brief mixing. NP signal in each fraction was monitored using a modified iodine assay, and BayK presence was determined by measuring each fraction's absorbance at 415 nm. (G) NP hydrodynamic diameter before and after BayK loading, measured by light scattering. (H) In vitro release profile of BayK from BayK-NP at room temperature (RT) and 37°C ($n = 3$). Loss of free BayK through the membrane is also shown. (I) BayK encapsulation efficiency when mixed with NP (30 mg/ml). a.u., arbitrary units.

with BayK-NP reduced contraction frequency, increased contraction amplitude, and resulted in an overall improvement in vessel pumping efficiency as measured by the ejection fraction (Fig. 2G). Previous studies have shown that pumping frequency does not affect LV pressure generation, except at extremely low frequencies (42). Thus, although BayK-NP application reduced LV contraction frequency, accompanying increases in amplitude and ejection fraction could be sufficient to improve overall vessel function and pressure generation. Incubation with free BayK increased both the amplitude and the ejection fraction, results consistent with the effects of the BayK-NP formulation, whereas control NP treatment did not affect any function metrics. Together, these data indicate that BayK's effects on improving LV pumping *ex vivo* are maintained when delivered into LVs encapsulated within the NP.

Locoregional administration of BayK-NPs acutely enhances the pump function of draining LVs

With evidence that BayK's improvement of pumping function in isolated vessels was maintained in the BayK-NP formulation, formulation influences on vessel function *in vivo* were evaluated. Upon tail tip injection of IRDye 800CW-labeled 20-kDa PEG tracer, collecting LVs in the tail could be immediately and clearly imaged by NIR microscopy (Fig. 3A). Because PEG does not associate with NP upon mixing (fig. S3A), simultaneous injection with NP is not expected to affect lymphatic drainage of the PEG fluorescent tracer, and therefore, the pump function metrics were calculated on the basis of tracer transport. Vessels were imaged from the left or right side of the tail, and tracking fluorescent intensity at a region of interest revealed clear contraction peaks, consistent with the movement of lymph in "packets" (Fig. 3A and fig. S3B). These traces were then analyzed to yield several metrics of LV-pumping function, including packet frequency, packet amplitude (which

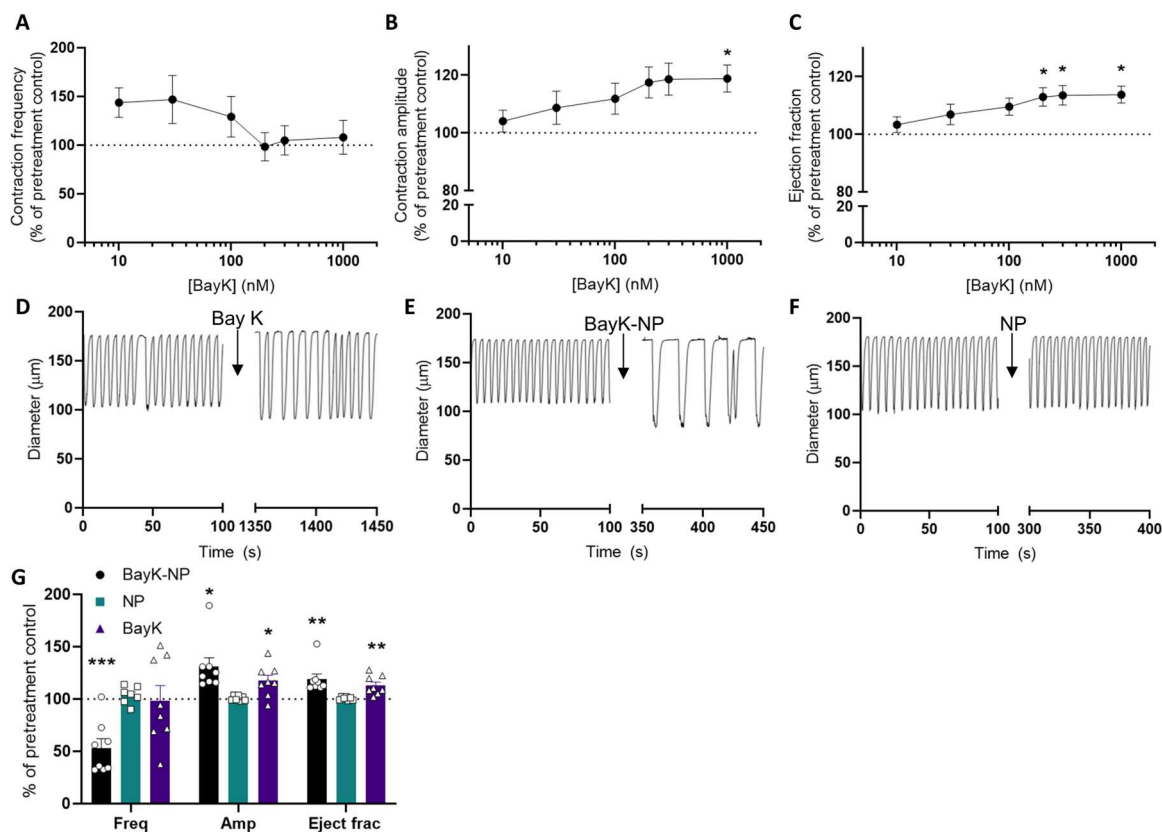


Fig. 2. Effect of BayK-NPs on ex vivo pumping of isolated rat mesenteric LVs. Contraction frequency (A), contraction amplitude (B), and ejection fraction (C) by LVs isolated from the rat mesentery after exposure to BayK. Asterisk indicates statistically significant difference compared to pretreatment 100% function by one-way repeated-measures analysis of variance (RM ANOVA) ($n = 8$). (D) Representative recordings of spontaneous contractions in an isolated LV ex vivo before and after treatment with 200 nM BayK, (E) 200 nM BayK-NP, or (F) dose-matched control NP. (G) Change in vessel contraction frequency, amplitude, and ejection fraction after treatment with NP, 200 nM BayK-NP, or 200 nM BayK. Presented as normalized to pretreatment baseline. Asterisk indicates significant difference between treatment value and a pretreatment value of 100% by t test with Holm-Sidak correction ($n = 7$ to 8). In all panels, $*P < 0.05$, $**P < 0.01$, and $***P < 0.001$.

correlates with contraction amplitude), packet integral (which correlates with stroke volume), and packet transport (which correlates with the amount of fluid pumped per minute by contraction), a critical metric of vessel function (40). To investigate the effect of both free and NP-encapsulated BayK on vessel function in vivo, vessels were imaged following a tail tip injection containing 80 μg of BayK in 50% dimethyl sulfoxide (DMSO), 50% DMSO, BayK-NP loaded with 80 μg of BayK, or dose-matched NP with no drug loaded. While BayK administration did not affect vessel pumping by any functional metric immediately after treatment (0 hours) compared to the DMSO vehicle control (Fig. 3, B to E), BayK-NP increased packet amplitude, packet integral, and packet transport compared to its NP vehicle control (Fig. 3, C to E). An immediate decline in pumping frequency was also observed with BayK-NP treatment (Fig. 3B); this is consistent with the reduction in pumping frequency and increase in amplitude and overall fluid transport seen with BayK treatment in the literature (27) and in isolated vessel experiments (Fig. 2G). Consistent with the interpretation of ex vivo results, these measurements suggest that the reduced contraction frequency does not prevent improvement in lymph transport by more direct metrics, similar to packet transport, potentially due to the low impact of contraction frequency on vessel pressure generation capabilities (42). Following functional imaging immediately

after treatment, mice were again imaged at either 8 or 15 hours later; only one additional time point was used per animal to avoid potential effects of repeated NIR tracer injection on treatment clearance from the tail tip. Eight hours after BayK or BayK-NP application, no changes in pumping frequency were observed (Fig. 3B). However, BayK-NP treatment uniquely increased packet integral and trended toward increasing amplitude compared to control NP, while administration of BayK in its free form had no such effects (Fig. 3, C and D). By 15 hours after treatment, effects of a single BayK-NP injection were no longer observed (Fig. 3, B to D). These results highlight the importance of lymphatic access to enable BayK efficacy in vivo; functional improvement was only observed when BayK was formulated into a NP, while free BayK had no effect. These results also suggest that a single BayK-NP injection has lasting effects on vessel function that persist for at least 8 hours but which diminish within 15 hours.

BayK off-target effects are ameliorated by lymph-draining NP formulation

Because of BayK's hydrodynamic small size, it is expected to rapidly access circulation upon injection in peripheral tissues. This was confirmed by measuring the concentration of BayK in blood following tail injection of BayK or BayK-NP. Free BayK was observed to

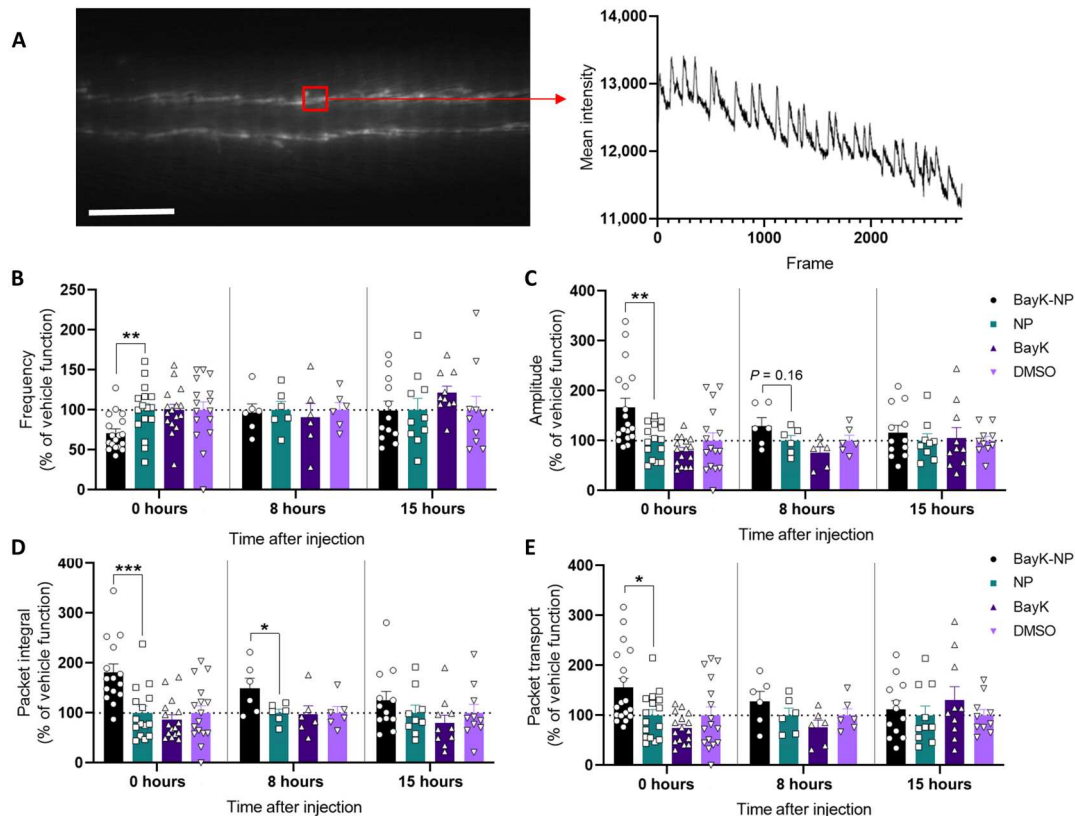


Fig. 3. NP-formulated BayK, but not free BayK, acutely improves lymphatic pumping in vivo. (A) Representative NIR image of LVs and resulting fluorescent intensity trace. Vessels are imaged from the left or right side of the tail. Regions of interest are selected on visible vessels, and fluorescent intensity traces are analyzed to obtain pumping metrics. Scale bar, 2 mm. (B) Packet frequency, (C) normalized packet amplitude, (D) normalized packet integral, and (E) normalized packet transport immediately after (0 hours), 8 hours after, and 15 hours after tail tip injection of BayK, BayK-NP, or their vehicle controls (DMSO and NP, respectively); all metrics presented as separate left and right vessels normalized to respective vehicle controls. Outliers were identified by ROUT (robust regression and outlier removal, $Q = 1\%$) and removed before analysis. Significance tested by unpaired t tests between BayK formulation and appropriate vehicle control. In all panels, * $P < 0.05$, ** $P < 0.01$, and *** $P < 0.001$.

access the blood within minutes, resulting in a significantly higher acute blood concentration than the same dose of BayK when formulated within the NP (Fig. 4A). This rapid systemic access may contribute to known side effects of BayK administration, including altered heart rate (43), motor impairment, and behavioral changes (34, 44). While no clear effect of BayK administration on mouse heart rate, as measured by pulse oximeter in anesthetized mice, was observed (fig. S4), potentially because of the overwhelming effect of anesthesia, free BayK administration did result in more severe side effects than the same dose of BayK-NP (Fig. 4, B and C). While BayK-NP caused minor side effects, such as hunching, excessive grooming, or impaired motor coordination, mice given free BayK showed more severe side effects and significant mobility challenges (Fig. 4C). NP delivery thus not only enables lymphatic uptake of a typically ineffective small molecule but also significantly reduces drug side effects by preventing rapid drug access to circulation and providing gradual release.

To investigate the systemic effects of chronic BayK-NP administration, mice were treated daily with BayK-NP for 11 days. Mice were then euthanized, and serum and spleens were harvested for analysis. Although NP-sized molecules are cleared primarily by the liver (29), no evidence of liver toxicity was observed after daily BayK-NP treatment for 11 days; alanine transaminase (ALT)

and aspartate aminotransferase (AST) levels were unchanged compared to NP or untreated controls (Fig. 4, D and E). Spleen mass was also unchanged by BayK-NP treatment (Fig. 4F), suggesting that chronic BayK-NP administration does not induce systemic immune side effects.

Because BayK activates calcium channels that play an important role in immune cell function (45, 46) and immune infiltration and dysregulation is critical in lymphedema development and progression (17), the effect of BayK on T cell activation in vitro was evaluated (fig. S5). As a positive control, when murine splenocytes were treated for 4 hours with phorbol myristate acetate (PMA) and ionomycin, there was a clear up-regulation of immune markers in both $CD4^+$ T cells (CD69 and PD-1) and $CD8^+$ T cells (CD25, CD69, and PD-1). Although BayK can activate similar pathways with a high enough concentration, treatment with BayK (0.9 $\mu\text{g}/\text{ml}$) for 4 hours did not induce any increase in expression of these markers (fig. S5, B and C), and T cell viability and regulatory T cell frequency were similarly unaffected (fig. S5, D and E). This suggests that BayK may be applied in vivo at the amount explored herein without overt direct immune modulatory effects on T cells.

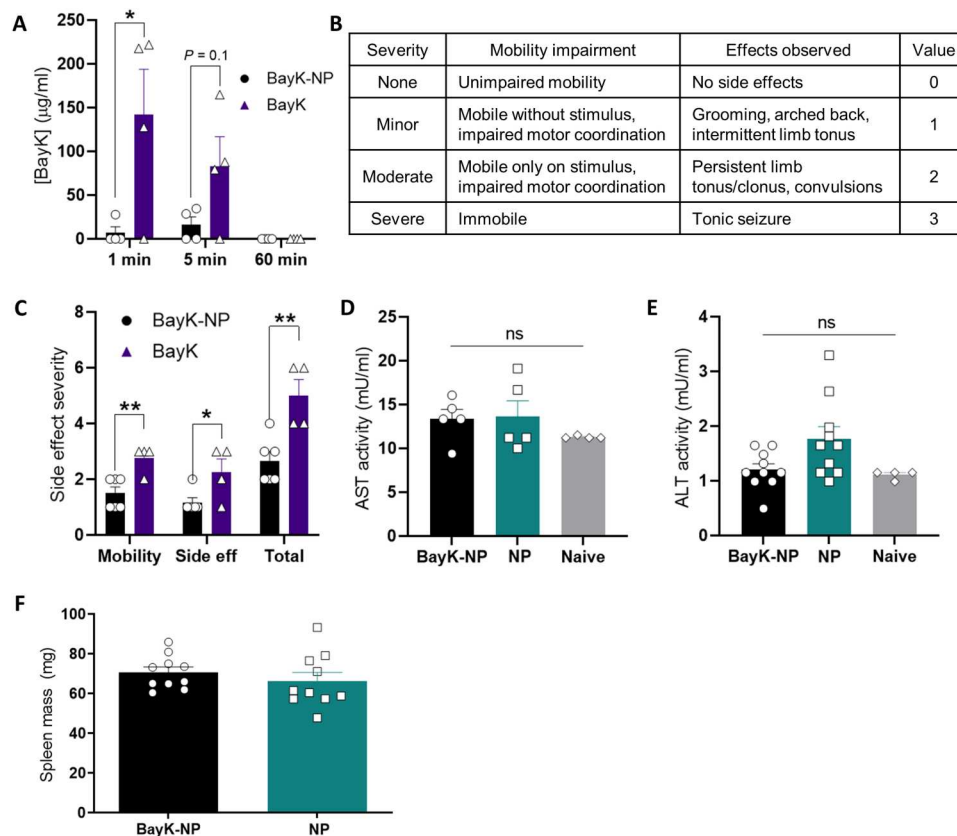


Fig. 4. BayK-NP show reduced side effects and toxicity compared to free drug. (A) Concentration of BayK detected in blood after tail injection of BayK-NP or free BayK. Asterisk indicates significant difference by *t* test. (B) Side effect severity scale. (C) Quantification of observed side effects. Asterisk indicates significant difference by *t* test. (D) AST and (E) ALT activity in serum. In (D) and (E), differences were evaluated by one-way ANOVA with Tukey's post hoc analysis ($n = 4$ to 10). (F) Spleen mass after chronic BayK-NP treatment. Differences tested by *t* test ($n = 10$). In all panels, $*P < 0.05$ and $**P < 0.01$. ns, not significant.

Single vessel ligation lymphedema model demonstrates tail swelling and impaired LV-pumping function

To evaluate the effect of BayK-NP in a model of lymphatic dysfunction, a single LV ligation model was used in which the dominant collecting vessels of the tail are ligated by cauterization along with superficial lymphatic capillaries around the circumference of the tail, leaving only a single collecting vessel intact (40, 47), mimicking lymphatic injury after cancer treatment in which intact functional vessels are usually present during lymphedema (Fig. 5A) (48). This surgery resulted in immediate cessation of flow-through ligated vessels but still allowed drainage past the ligation site in intact vessels (Fig. 5B). Tail swelling was consistently observed, as indicated by an increase in tail diameter immediately distal to the wound following surgery, peaking uniformly for animals by day 7 (d7) and either remaining steady or subtly attenuating (Fig. 5, C and D). This swelling was accompanied by significantly impaired pumping function in the intact lymphatic collectors by every metric, including contraction frequency, amplitude, and packet transport at d7, and packet integral and packet transport at d14 after surgery (Fig. 5E). There was additionally a significant correlation between amplitude and tail diameter and between packet transport and diameter and nonsignificant correlations in frequency and packet integral (Fig. 5F), suggesting that function by these metrics decreases with increasing tail diameter as has been shown previously (40). In

addition, at both 7 and 14 days after surgery, vessel pumping pressure was lost (Fig. 5E), although the pumping pressure before surgery was measurable in all mice at 20.5 ± 8.4 mmHg. Clearance from the tail was also impaired. When fluorescently labeled dextran and NP, both 30 nm in hydrodynamic diameter, were injected in the tail tip 12 days after surgery, signals for both were increased in tails in which an LV had been ligated (lymph) compared to wild-type (WT) healthy tails wherein no LV ligation occurred (Fig. 5G) because of accumulation distal to the ligation as measured by IVIS (In Vivo Imaging System) (Fig. 5H). This reduced clearance resulted in significantly reduced accumulation of both dextran and NP in sacral LN-draining ligated vessels compared to those draining intact vessels (Fig. 5I), although no significant difference between dominant and nondominant-draining sacral LNs was observed in WT animals. Note that during the course of experiments, the ligated lymphatic collectors remained occluded, but the intact collectors remained patent; injected NP could produce clearly visualized drainage past the ligation site in the intact vessel even 14 days after surgery (Fig. 5J). The single-vessel ligation model is thus well suited for investigation of BayK-NP application, as an intact vessel still remains available for drug efficacy, recapitulating human disease in which secondary lymphedema can result despite incomplete disruption of vessels within a drainage bed.

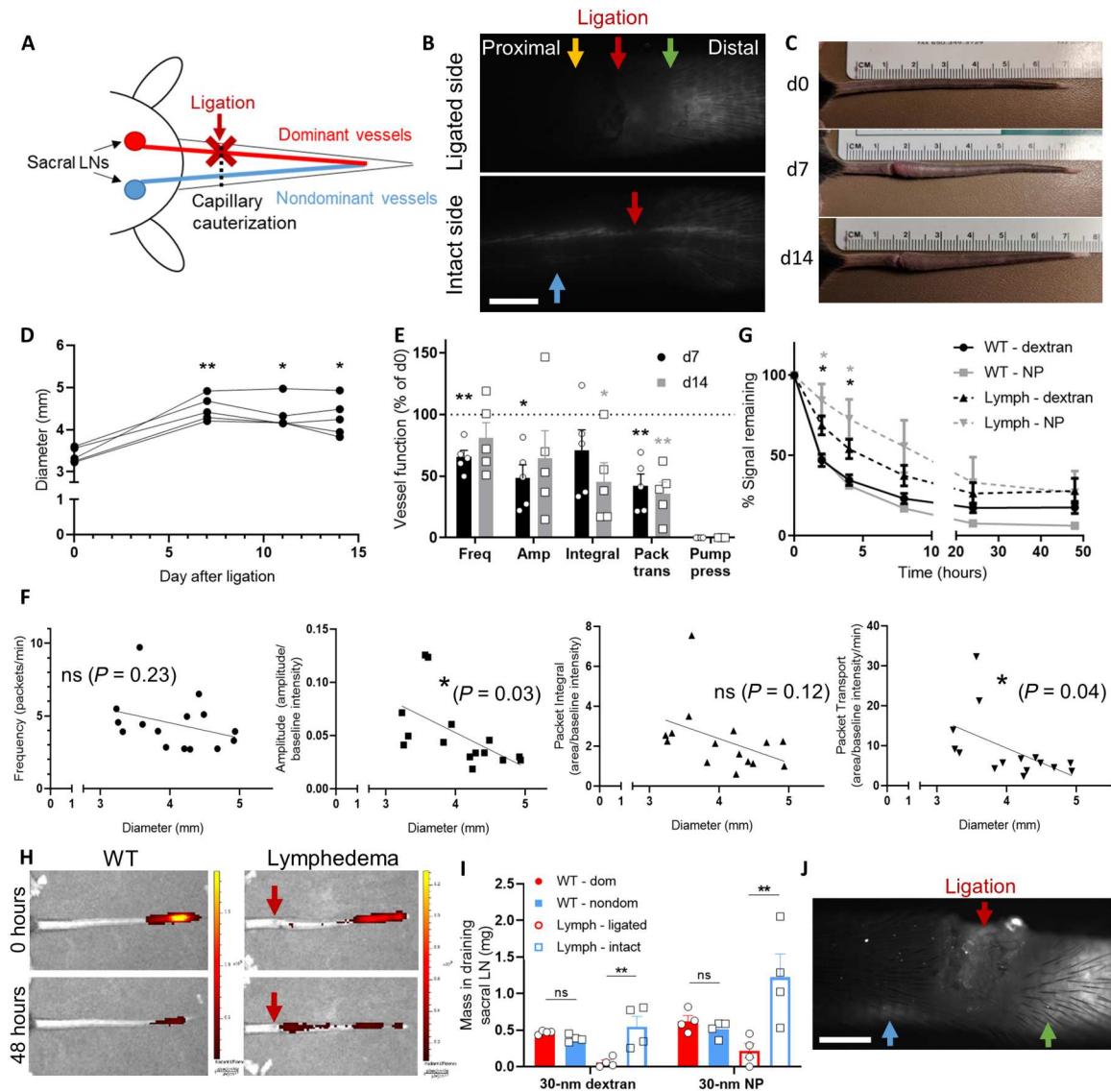


Fig. 5. The single vessel ligation lymphedema model shows dysfunction in intact LVs. (A) Schematic of surgical induction of lymphedema. (B) Surgery allows flow through the intact, but not ligated, LVs. Red arrow, ligation; yellow arrow, no flow past ligation; green arrow, dye accumulation distal to ligation; blue arrow, dye flow past ligation. Scale bar, 2 mm. (C) Representative tail images on d0 (before surgery), d7, and d14. (D) Tail diameter distal to ligation in individual mice following surgery. Asterisk indicates difference from d0 by one-way RM ANOVA. (E) Vessel function after surgery. One pumping pressure outlier was identified by ROUT ($Q = 1\%$) and removed before analysis. Asterisk indicates difference from d0 100% function by one-way RM ANOVA. (F) Vessel function metrics correlated with tail diameter. (G) Fluorescence signal in the tail after tail tip dextran or NP injection, quantified from IVIS images. Asterisk indicates difference between no disease WT and lymphedema (lymph) surgery animals by two-way RM ANOVA. (H) Representative IVIS images of tails after 30-nm dextran injection. (I) Dextran and NP accumulation in individual sacral LNs in WT and lymphedema surgery mice. Asterisk indicates difference by one-way ANOVA with Tukey's comparison. (J) NIR imaging of 680-NP uptake into LVs on d14, top view. Blue arrow, NP flow past ligation site; green arrow, distal accumulation. Scale bar, 2 mm. In all panels, $*P < 0.05$ and $**P < 0.01$.

Locoregionally administered BayK-NPs improve LV pump function in lymphedema model

Working within the single vessel ligation model (Fig. 5), mice were then treated daily with 68 μg of BayK-NP or control NP starting d3 after surgery through d14. Mouse behavior was assessed following injection at d3 after surgery, and daily tail swelling measurements and lymphatic functional imaging were performed on d0 (presurgery), d7, and d14. Similar to what was observed in healthy mice, BayK treatment resulted in higher side effect severity than BayK-NP treatment in mice with lymphedema (Fig. 6A). Frequency,

amplitude, and packet transport that were reduced after ligation also remained unchanged by BayK and BayK-NP treatment compared to their vehicle controls (figs. S6, A to F, and S7, A to F). Despite no differences in other functional metrics, pumping pressure at d14 was notably increased for BayK-NP-treated mice relative to those treated with free BayK or the NP vehicle (Fig. 6B), a distinction highlighted by the BayK-NP treatment having a greater likelihood of restoring pumping pressure than all control groups (Fig. 6C). Although no changes in tail swelling were seen with treatment, lymphedema is associated with chronic remodeling of

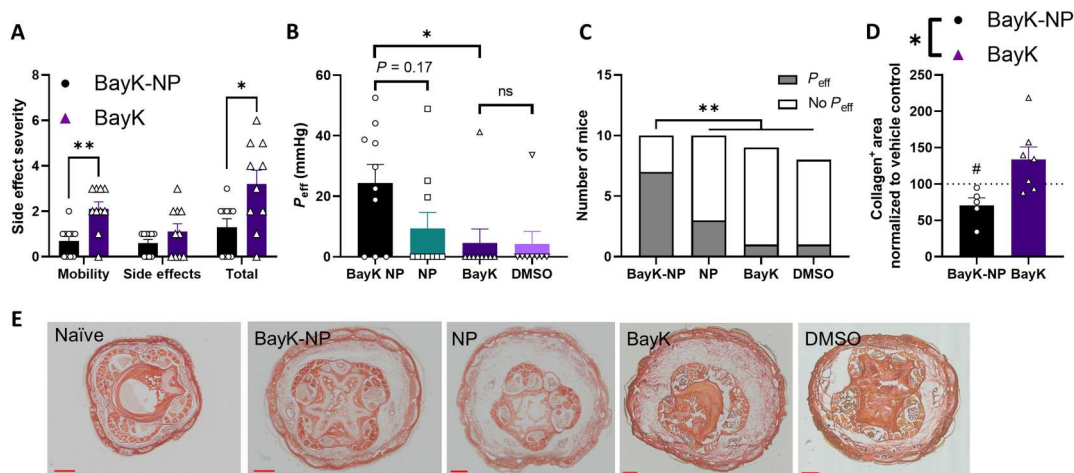


Fig. 6. BayK-NP treatment protects against lymphatic pumping pressure failure in lymphedema. (A) BayK side effects in lymphedema mice immediately after treatment were significantly reduced by NP formulation. (B) Mice treated with BayK-NP had significant improvement in pressure generation 14 days after injury compared to treatment with free BayK. (C) A greater proportion of mice maintained measurable pumping efficacy 14 days after injury when treated with BayK-NP rather than free BayK. Statistical significance determined by Fisher's exact test comparing BayK-NP effect to combined effect of control groups. (D) Quantification of collagen⁺ area between the muscle fascia and dermis for BayK treatments normalized to respective vehicle control. Number sign indicates significantly lower collagen deposition relative to vehicle control by *t* test against normalized control; asterisk indicates significantly stronger effect relative to vehicle control than observed from free BayK formulation. (E) Sirius Red staining for collagen in mouse tail sections 14 days after lymphedema induction. Scale bars, 500 μ m. In all panels, **P* < 0.05 and ***P* < 0.01.

affected tissue (19, 49, 50). The effect of BayK treatment on tissue structure in swollen tails d14 after surgery was thus assessed. Staining sections with Picro-Sirius Red for collagen imaging revealed increased collagen deposition in lymphedematous tails compared to naïve animals, consistent with previous studies (51, 52), that was reduced with BayK-NP, but not BayK, treatment (Fig. 6, D and E, and fig. S8), suggesting that delivery of BayK into lymph enabled by the NP formulation can inhibit the remodeling associated with lymphedema progression. BayK-NP treatment did not, however, alter skin thickness (fig. S9, A to C) or average LV area (fig. S9D) as measured in hematoxylin and eosin (H&E)-stained sections (fig. S10). These results suggest that NP enable the therapeutic effects of BayK to be safely realized with respect to improving lymphatic pump function in the context of lymphedema, effects associated with reduced collagen accumulation.

DISCUSSION

Collecting LVs are attractive therapeutic targets because of the important role of LV function in a variety of pathologies including heart disease, obesity, and lymphedema. However, no pharmacologic approaches have been developed to enhance lymphatic pumping *in vivo*. This is likely because delivering agents to LMCs to improve the function of collecting LVs presents numerous delivery challenges. First, administered drugs typically have poor access to lymphatic tissues from the systemic circulation. Hence, locoregional routes of administration offer advantages with respect to providing an administered therapeutic access to local collecting LVs draining the injection site. This is because after drainage into LVs, lymph-borne agents have improved access to LMCs that surround the LV wall just outside the lumen. Second, small-molecule drugs, which represent a large number of potential therapeutics investigated to date that target pathways regulating LV function (28, 53–55), show poor accumulation within lymph after locoregional

administration due to their short half-life of tissue retention and rapid clearance via blood capillaries (36, 37). To overcome this limitation, a variety of controlled delivery and release technologies have been used to improve lymphatic uptake of drug payloads (35, 38, 39, 56, 57). The biomaterial NP platform used in this work is a versatile system well suited for the application; the NPs are modular, composed of nontoxic, biocompatible polymers, can encapsulate and release hydrophobic drug without the need for chemical modifications or environmental stimuli and have been previously shown to improve the delivery of small molecules to lymphatic tissues (30, 35, 39, 58). Notably, however, all approaches to date that harness controlled delivery and release approaches to increase lymphatic uptake do so with the intent to target the LN and the immune cells resident there. The work described here represents a logical extension of this idea, taking advantage of enhanced lymphatic drainage to target LVs themselves rather than their downstream LNs.

Administered small-molecule BayK was found to only be capable of improving the pumping function of draining LVs when in delivered in a NP formulation. This highlights the importance of lymphatic uptake for vessel-targeting drug efficacy. Notably, BayK acts on L-type calcium channels expressed on LMCs rather than acting directly on the lymphatic endothelial cells that line the vessel lumen. BayK may reach these target cells by diffusion from the vessel lumen after intraluminal release from the NP vehicle, as LV walls are relatively thin, or could be released during NP degradation if NPs are taken up by phagocytic lymphatic endothelial cells. Regardless of the mechanism, the observed efficacy of a drug that acts on LMCs suggests that a bioactive drug concentration is achieved at LMCs after intraluminal accumulation, a promising result for delivery of other contractility-modulating drugs. The NP delivery vehicle used in this work is a versatile platform that could be easily extended to deliver other hydrophobic drugs or modified on the NP corona to deliver hydrophilic agents

and applied for drug delivery to lymphatic endothelial cells as targets or LMCs as explored here.

In addition to improving LV pumping function *in vivo*, BayK-NP also reduced the severity of side effects observed after BayK administration (Figs. 4C and 6A). Targeted or controlled drug delivery, including using NP platforms, has long been lauded as a method to increase drug concentration at the target site, allowing for lower or less frequent dosing while reducing systemic drug concentration and resulting to off-target effects. BayK-NPs are no exception and provide these advantages. Upon injection into the interstitium, small molecules diffuse quickly into the blood circulation, where they typically have short half-lives and are cleared rapidly by the kidney (29). In the case of BayK, this results in a rapid but brief spike in the concentration of drug in the blood (Fig. 4A). Because L-type calcium channels are expressed on a variety of off-target cells, this exposure results in substantial side effects; at their most severe, animals would become nonresponsive and show involuntary muscle contractions. BayK-NP likely reduces BayK concentration in the blood in several ways. First, NPs are cleared slowly from the site of injection, draining into lymph gradually. Simultaneously, BayK-NPs do not release their entire BayK payload immediately upon injection; rather, the payload is released over the course of several days (Fig. 1H). While BayK released from BayK-NP, whether at the injection site or after lymphatic drainage, can still eventually access the blood, the reduced side effects associated with the NP formulation may be due to the measured drug release that keeps the concentration from spiking. Future work can further explore these benefits of BayK-NP administration and can investigate the lowest effective BayK-NP dose to further reduce toxicity.

Animal models of lymphedema development are currently limited. Models including rabbit ear and dog hindlimb models, in which LVs are disrupted and tissue was removed to halt flow and induce pathological swelling, have been investigated but suffer from complexity and inconsistency (59, 60). Although LN removal models are analogous to LN resection surgeries that often precede lymphedema in human patients, these animal models suffer from similar inconsistencies and are additionally disadvantageous because of the lack of any intact draining LNs, something that does not occur in human patients because of the much larger abundance of LNs. A commonly used model is the rodent tail model (23, 61, 62), in which all initial and collecting LVs in the tail are severed, resulting in swelling, immune infiltration, and tissue remodeling. This double vessel ligation model has been used in many lymphedema studies focused on characterizing the morphological changes associated with disease progression, for which it is well suited. The model has also been used to investigate lymphedema treatment by targeting immune regulation or lymphangiogenesis; total cessation of lymph flow out of the tail induced by severing LVs around the full tail circumference provides an excellent environment to study the ability of lymphangiogenesis to bridge the gap and restore lymph drainage. This model has limited application in studies of collecting LV-pumping function, however, as it leaves no collectors intact for analysis or to therapeutically target. For this reason, in this study, a lymphedema model was used in which the dominant collecting LVs and superficial lymphatic capillaries in the mouse tail were selectively cauterized (40), leaving nondominant collecting LVs intact (Fig. 5J) but with reduced pumping function (Fig. 5E). These intact collectors are the target of the BayK delivered

in this study, as they are capable of taking up the injected NP and productively responding to BayK to improve pumping function, unlike completely severed and occluded vessels. In addition to being well suited for investigations of BayK administration and LV function modification, this model is arguably more representative of the human case, in which secondary lymphedema can result from incomplete disruption of vessels from a drainage bed (48), and shows similar swelling and morphological changes compared to the double vessel ligation model (40). Although the single vessel ligation model does not perfectly mirror the chronic, life-long course of swelling often observed in human patients, the simplicity, consistent tail swelling, and impaired function of intact collectors make this model highly valuable for investigations of collecting vessel function modulation.

Daily treatment with BayK-NP improved several metrics of lymphedema progression. The most important data relevant to the therapeutic approach explored herein are the d14 increase in LV pressure generation, a metric of vessel function associated with reduced swelling (21). Collagen deposition, which is often observed in lymphedema and associated with swelling (50), was also reduced in swollen tail tissue at d14 after surgery, suggesting less severe disease with BayK-NP treatment. As lymphedema is a complex disease without a single defined metric for disease resolution, the observed improvement in each of these metrics associated with disease is promising. However, no overall changes in tail swelling with treatment were measured. It is likewise important to interpret this result in light of this animal model, in which the swelling will resolve on its own without intervention if given enough time (40). The observation that BayK-NP sustained LV pump function is an important finding and provides the first evidence to our knowledge that a medicinal approach to directly enhancing LV contractility has efficacy in reducing pathology in a lymphedema model. The fact that improved LV function at d14 was not associated with a further reduction in tail swelling may suggest that by d14, other factors affecting lymphedema progression overwhelm the benefit of improved LV pumping alone or that pathways leading to its resolution are occurring simultaneous with those of the BayK-NP. Immunological changes, for example, play an important role in lymphedema development (17, 18, 47, 63, 64). Further, in double vessel ligation models, dermal lymphatic endothelial cell proliferation has been observed to occur within 2 weeks after ligation surgery (61). If lymphangiogenesis begins to occur naturally during disease resolution, it may reduce the benefit of improved vessel pumping function at later time points.

This work represents, to our knowledge, the first attempt to alleviate lymphedema symptoms by directly targeting LV-pumping function and reveals the potential of such an approach as it is a critical first step for innovating therapeutic approaches that improve LV pump function, which could augment lymphangiogenic therapy. These results also highlight the complexities of lymphedema development and the many opportunities for further development of engineered drug delivery systems to enhance LV pumping function. For example, a single injection of BayK-NP was found to improve pumping function after 8 hours, but the effects were lost after 15 hours. This short window of efficacy necessitated repeated injection of BayK-NP for treatment of chronic swelling. Future work should investigate the long-term effects and feasibility of this repeated dosing and evaluate whether repeated dosing has additive effects on vessel function improvement. Additional benefits of treatment

including enhanced efficacy reduced dosing frequency, and improved translatability could also be achieved by slowing the time-scale of release for more sustained effects with fewer administrations. To maximize benefit, future approaches could also use combination therapies to simultaneously address lymphatic function, lymphangiogenesis, and immune modulation.

In summary, a lymph-draining NP platform was leveraged for the delivery and release of small-molecule drug BayK 8644 into LVs at functional concentrations. By using NIR microscopy to image pumping function of mouse tail collecting LVs in vivo in real time, treatment with BayK-NP was found to significantly improve LV pumping function, with effects lasting ~8 hours, while injection of free small-molecule BayK could not elicit these effects. The NP formulation also lowered BayK concentration in the blood and reduced the severity of side effects observed because of off-target BayK delivery compared to the small-molecule formulation. BayK-NP thus enabled BayK efficacy in vivo while simultaneously improving its safety. When applied to treat a murine model of lymphatic dysfunction in which tail lymphedema is induced by ligation of all tail LVs but nondominant collectors, BayK-NP increased LV pumping pressure in intact LVs compared to NP control and reduced collagen deposition. This work highlights the importance of lymphatic drainage in the efficacy of drugs that act on LVs and explores a lymph-targeting NP platform to achieve this lymphatic drainage. This also represents, to the best of our knowledge, the first evidence that directly promoting pumping function can ameliorate dysfunctional LV pumping in lymphedema, highlighting a promising approach to treating this complex disease with potential relevance to other lymphatic diseases.

MATERIALS AND METHODS

Study design

This study was designed to test the ability of BayK incorporated into a lymph-draining NP formulation to improve LV-pumping function and to subsequently test BayK-NP efficacy for the treatment of mouse tail lymphedema. In these controlled laboratory experiments, mice were injected in the tail tip with BayK formulations, and subsequent LV function was evaluated by NIR imaging. In lymphedema studies, animals were euthanized at a predefined d14 time point for tissue analysis. Mice were randomly assigned to treatment groups, with each cage having at least one mouse from each treatment group, and sample sizes were selected to achieve 80% power with minimal animal use based on previous experiments. Lymphedema experiments represent two repetitions of 10 mice each, and, for logistical reasons, LV function data represent four experiments of 6 to 12 mice each. Experiments were not performed in a blinded fashion. Statistical methods are described in the "Statistical analysis" section.

BayK-NP synthesis and characterization

NPs were synthesized as previously described (30). Briefly, 500 mg of Pluronic F127 was dissolved in 10 ml of degassed Milli-Q water under argon, and 400 μ l of propylene sulfide (TCL, Tokyo, Japan) was added. After 30 min, thiolated initiator (65) activated in sodium methoxide was added under argon and was allowed to react for 15 min under stirring. 1,8-Diazabicyclo[5.4.0] undec-7-ene (64 μ l) was added under argon, and the solution was capped

for 24 hours. The reaction was then exposed to air for 2 hours, and the resulting NP were dialyzed in a 100,000-Da membrane (Spectrum Labs, New Brunswick, NJ) against 5 liters of Milli-Q water for at least 3 days. In experiments where fluorescent NPs were required, NPs were reacted overnight at room temperature with a 6 M excess of Alexa Fluor 647 C₂ maleimide (Thermo Fisher Scientific, Waltham, MA) or with IRDye 680RD maleimide (LI-COR, Lincoln, NE), and unreacted dye was removed by size exclusion chromatography on a CL-6B resin.

NPs were loaded with BayK by mixing BayK (1 mg/ml; Cayman Chemical, Ann Arbor, MI) with NPs (7.5 to 30 mg/ml) in 5% tetrahydrofuran for 5 min, and unencapsulated BayK was removed by cleaning on a 7-kDa Zeba column (Thermo Fisher Scientific). To verify successful encapsulation, uncleaned BayK-NP were run on a CL-6B size exclusion column, and BayK association with NP was evaluated by measuring BayK absorbance at 415 nm and NP signal using a modified iodine assay that detects the presence of Pluronic (PEG) (30) in each fraction using a Synergy H4 BioTek plate reader. To determine BayK encapsulation efficiency, BayK-NP was cleaned of unencapsulated drug as described, then lyophilized, and resuspended in acetonitrile. The amount of BayK was determined by comparing the solution absorbance at 415 nm to a standard curve, and the encapsulated drug concentration was compared to the originally added dose. BayK release from NP was evaluated by dialyzing BayK-NP in a 3.5-kDa membrane and monitoring solution absorbance over time. NP size was measured before and after BayK loading by dynamic light scattering on a Malvern ZetaSizer instrument.

Isolated vessel studies

To evaluate the effect of BayK and BayK-NP directly on collecting LV pumping, mesenteric LVs were extracted from male Sprague-Dawley rats as described by Davis *et al.* (66). A 1-cm segment of vessel was submerged in 37°C physiological salt solution (PSS, consisting of 145.0 mM NaCl, 4.7 mM KCl, 2.0 mM CaCl₂, 1.17 mM MgSO₄, 1.2 mM NaH₂PO₄ mM, 5.0 mM dextrose, 2.0 mM sodium pyruvate, 0.02 mM EDTA, and 3.0 mM Mops) and cannulated in an ex vivo lymphatic perfusion system as previously described (67, 68), allowing for precise maintenance of transmural pressure at 3 cmH₂O throughout the course of the experiment. Contractions of the vessel were imaged using a bright-field camera at 30 frames/s (fps), and vessel diameter was calculated using a custom LabView program. After allowing vessel segments to equilibrate in 37°C PSS for 15 min, vessel function was verified by applying incremental pressure steps at 3, 2, 1, 0.5, 3, 5, 8, 10, and 12 cmH₂O for 3 min each to ensure that the vessel was not damaged during cannulation and that normal transmural pressure-dependent changes in lymphatic contractility were observed, as has been reported previously (69). Baseline, or pretreatment, function for each vessel was obtained by imaging for 3 min before the addition of treatment. The dose-dependent effect of BayK was tested by incrementally adding 10, 30, 100, 200, 300, and 1000 nM BayK into the vessel bath for 5 min each, while continuously monitoring vessel diameter. To evaluate the effect of BayK-NP on vessel pumping, vessel segments were sequentially treated with a low dose of NP for 5 min, a high dose of NP for 40 min, a low dose of BayK-NP (200 nM) for 5 min, and a high dose of BayK-NP (1000 nM) for 40 min. High- and low-dose NP treatments were dose-matched to BayK-NP treatments, providing a control for the intrinsic effects of the NP vehicle. In some

vessels, pressure step testing was repeated in the last 30 min of high NP and high BayK-NP dose treatment to determine whether treatment altered the pressure response. Any time pressure steps were applied, the vessel was allowed to equilibrate for 30 min for contractile function to return to baseline. At the end of each vessel segment experiment, the physiological salt solution bath was replaced with a calcium-free solution to induce maximal relaxation of the lymphatic muscle, and the vessel was imaged for an additional 5 min, providing resting diameter information and allowing calculation of vessel tone. Vessel functional metrics were calculated from vessel diameter traces using a custom MATLAB script. Parameters include frequency (the average number of contractions per minute), end diastolic diameter (EDD), end systolic diameter (ESD), amplitude (the average change in vessel diameter in one contraction, $EDD - ESD$), ejection fraction [$(EDD^2 - ESD^2)/EDD^2$], and fractional pump flow (frequency \times ejection fraction) (25).

In vivo function analyses

Mice were anesthetized with inhaled isoflurane (1.8% maintenance) and injected with 10 μ l of IRDye 800CW-labeled 20-kDa PEG tracer intradermally at the midline of the tail, less than 1 cm from the tail tip. Before imaging, 5 min was allowed for flow to normalize and for signal to appear in LVs along the entire length of the tail. Vessels were then imaged using NIR microscopy as previously described (40, 70). Briefly, the system consisted of an MVX-ZB10 microscope (Olympus), a Lambda LS xenon arc lamp (Shutter Instruments), a 769-nm bandpass excitation filter, an 832-nm emission bandpass filter, and an Evolve Delta 512 electron-multiplying charge-coupled device camera (Photometrics). After allowing 5 min for dye to enter LVs, the mouse was placed on its side, and left side vessels were imaged for 5 min; the mouse was then placed on its other side, and right side vessels were imaged for an additional 5 min. Imaging was performed 1.6 cm from the tail base, using a 50-ms exposure time and a 10-fps frame rate. In some experiments, the pumping pressure was measured as previously described (40). Briefly, a pressure cuff was placed around the tail at 1.8 cm from the base of the tail. The pressure was quickly increased to 80 mmHg, held for 5 min to allow flow cessation, and then reduced to 55 mmHg. The pressure was then reduced in 2.5-mmHg increments, with each step held for 5 s, until a pressure of 0 mmHg was reached. During the pressure application, fluorescence intensity was imaged immediately proximal to the pressure cuff. Pumping pressure was defined as the pressure at which fluorescence intensity in the vessel recovered to 50% of its maximum after flow cessation and was calculated using a custom MATLAB script.

Functional pumping metrics, including packet frequency, packet amplitude, packet integral, and packet transport, were calculated from fluorescence images as previously described (40). Briefly, a series of fluorescent images was imported into ImageJ (National Institutes of Health, Bethesda, MD), and fluorescent signal over time for a region of interest was exported. The resulting intensity trace was analyzed using a custom MATLAB script to identify packets, or normal or inverse deviations from the fluorescence baseline, and to calculate functional metrics. Packet frequency is calculated as the number of packets that occurred per unit time. Packet amplitude is the change in fluorescence intensity between the packet minimum and maximum. Packet integral is the fluorescence signal within each packet or the area contained between the packet and baseline. Packet transport is the time-normalized sum

of all packet integrals in a video; it represents the total fluorescence signal moving through the vessel and is thus a metric of overall lymph transport due to intrinsic contractility of the LV. These metrics were individually evaluated for left and right vessels in each mouse. Amplitude, packet integral, and packet transport are presented as normalized to the vessel's baseline fluorescence to control for variations in vessel brightness between animals.

Lymphatic and off-target effects of BayK-NP treatment

To evaluate the acute and longitudinal effects of BayK and BayK-NP on lymphatic pumping in vivo, mice were simultaneously injected with IRDye 800CW-labeled PEG tracer and a treatment in a total volume of 18 μ l. Treatment groups included the following: 81 μ g of BayK in 50% DMSO, 50% DMSO (BayK vehicle control), BayK-NP containing 81 μ g of BayK, or dose-matched NP (BayK-NP vehicle control). All mice were imaged the day before treatment to establish baseline function and immediately after drug injection (0 hours) and were additionally imaged either 8 or 15 hours after injection to determine whether there was a sustained effect of treatment on LV function. All imaging was performed as described above and took less than 30 min to complete at each time point. During 0-hour imaging, mouse heart rate was monitored using a rodent pulse oximeter (Kent Scientific, Torrington, CT) clipped on the front left paw. After imaging was complete, mice were carefully observed, and the occurrence and severity of side effects and motor impairment were recorded. Motor impairment was characterized by unsteady movement or lack of movement, and other side effects included excessive grooming, hunching, limb tonus, shaking, or nonresponsiveness.

To investigate the role of BayK circulating in the bloodstream on the observed difference in side effect severity between BayK- and BayK-NP-treated mice, BayK concentration in the blood was measured after injection of either treatment in the tail tip in isoflurane anesthetized mice. Fifty microliters of blood was drawn by facial lancet before injection and at 1, 5, and 60 min after injection and was spiked with EDTA to avoid clotting. Fifty microliters of acetonitrile was added to precipitate blood proteins, and blood was then centrifuged at 20,000g for 20 min. Two microliters of the resulting supernatant was sampled in duplicate, and absorbance at 415 nm was measured on a plate reader using a Take3 plate. BayK concentration was calculated by comparison to a BayK standard curve.

Lymphatic ligation surgical model

C57/Bl6 mice were anesthetized with inhaled isoflurane (5% induction and 1.8% maintenance) and injected with 10 μ l of IRDye 800CW-labeled 20-kDa PEG tracer intradermally at the midline of the tail, less than 1 cm from the tail tip. Immediately after injection, the tail was imaged 1.6 cm from the tail base, and the dominant LV was determined by first appearance of fluorescent signal on the left or right side of the tail (71). The dominant side vessels were ligated by cauterization at 1.6 cm from the tail base. Superficial lymphatic capillaries were also cauterized by making a superficial ligation around ~90% of the tail circumference, taking care not to disturb the nondominant side lymphatic collectors. To verify successful surgery, NIR imaging was used to demonstrate complete cessation of flow-through ligated dominant vessels and to ensure that nondominant vessels remained intact. Antibacterial ointment was applied to the wound, and animals were given buprenorphine for pain management.

Lymphatic function and swelling progression in this lymphedema model were characterized in five mice over 14 days. On d0, pre-surgery imaging was performed on all animals, followed by immediate ligation of the dominant vessel and superficial lymphatic capillaries as described above. Functional imaging was additionally performed on d7 and d14 after surgery, and photos of the tail were taken on d0, d7, d11, and d14. From these photos, peak tail diameter was measured in ImageJ. On d12, five mice with lymphedema and five WT mice were injected with 23.8 μg of Alexa Fluor 610–labeled 500-kDa dextran (with a hydrodynamic diameter of 30 nm) and IRDye 680RD-labeled NP in a single, 15- μl tail tip injection. Fluorescent signal of both dextran and NP at the injection site was monitored using an IVIS imaging system at 0, 2, 4, 8, 24, and 48 hours after injection. After d14 functional imaging, mice were euthanized, and left and right sacral LNs draining the tail injection were separately harvested and homogenized in tubes prefilled with 1.4-mm zirconium beads (OPS Diagnostics, Lebanon, NJ). Dextran and NP fluorescence in the LN homogenate was measured using a plate reader.

Effects of BayK-NP treatment on vessel function and lymphedema development

Lymphedema was induced and treated in female C57/Bl6 mice. On d0, mice underwent vessel ligation surgery as previously described. Three days were allowed for wound healing and resolution of initial inflammation. Beginning on d3, mice received daily treatment by tail tip injection of either 67.5 μg of BayK-NP ($n = 10$), dose-matched unloaded NP ($n = 10$), 67.5 μg of BayK in 50% DMSO/50% saline solution ($n = 9$), or 50% DMSO/50% saline vehicle control ($n = 8$). Photographs of the tail were taken on d0 and daily beginning on d3 for swelling analysis in ImageJ. Functional imaging, including pumping pressure analysis, was performed on d0 (presurgery), d7, and d14. Because of large group sizes, imaging was staggered over multiple days. To account for day-to-day variability associated with a staggered procedure schedule, both treatment and vehicle control animals were included in any given surgical day. On d7, the daily treatment was given after imaging was complete to avoid measuring acute effects of the injection volume. After imaging was completed on d14, animals were euthanized, blood was collected by cardiac puncture into EDTA-coated tubes, spleens were harvested, and tail sections were collected for histology. Spleens were weighed and photographed. Blood was centrifuged at 2100g for 15 min, and the plasma supernatant was stored at -80°C until ALT and AST assays were performed according to the manufacturer's instructions (BioVision, Milpitas, CA).

To evaluate the effects of treatment relative to vehicle on tissue composition in the swollen region distal to the vessel ligation, histology was performed. For histology, 1 cm of tail distal to the ligation was fixed in 4% paraformaldehyde for 48 hours. Following fixation, samples from the BayK and DMSO treatment groups were frozen and cut into 5- μm sections, whereas for the BayK-NP and NP treatment groups, samples were decalcified in 0.5 M EDTA (pH 8) for 2 weeks, with EDTA changed two to three times per week, then paraffin-embedded, and cut into 5- μm sections. For H&E staining, slides were deparaffinized, hydrated by 15-min incubation in xylene, and washed in 100% alcohol, 95% alcohol, 70% alcohol, and water. Sections were stained with hematoxylin for 1 min; washed in acid alcohol, Scott's, and 95% alcohol; and then stained in eosin for 1 min. After sequential washes in alcohol and

xylene, slides were mounted in CytoSeal 60 (Thermo Fisher Scientific). For Picro-Sirius Red, slides were deparaffinized and hydrated, and nuclei were stained for 5 min with Weigert's hematoxylin. After washing, sections were stained for 1 hour in Picro-Sirius Red solution, washed in acidified water, dehydrated, and mounted. Epidermal thickness and dermal thickness were quantified from H&E images in ImageJ; each parameter was measured three times at representative locations around the tail circumference and averaged per section. Average LV area was quantified by tracing a minimum of 20 representative LVs in each section and averaging. In Picro-Sirius Red-stained sections, collagen⁺ pixels between the dermis and muscle fascia were quantified in ImageJ.

Immunological effects of BayK

To evaluate potential immunological effects of BayK administration, splenocytes were treated with BayK in vitro. A C57/Bl6 spleen was processed through a 0.7- μm cell strainer and treated with ACK lysis buffer to lyse red blood cells. Splenocytes were plated at 1 million cells per well in a 96-well plate, with 150 μl of RPMI medium. Splenocytes were treated with BayK (0.9 $\mu\text{g}/\text{ml}$; 2% of the in vivo dose and a feasible resulting LN concentration), PMA (20 ng/ml), and ionomycin (1 $\mu\text{g}/\text{ml}$; a positive control known to result in T cell activation) or DMSO (vehicle control). After 4 hours of incubation at 37°C , cells were washed and treated with 2.4G2 Fc block for 5 min on ice. Cells were then stained with the Zombie Aqua Fixable Viability Kit (BioLegend, San Diego, CA) for 30 min at room temperature and then stained for 30 min on ice with a panel of antibodies, including PerCP CD45, BV711 CD3, phycoerythrin (PE)/Cy7 CD4, fluorescein isothiocyanate CD8, Alexa Fluor 700 CD25, BV421 CD69, Alexa Fluor 647 PD-1, and PE FoxP3, all from BioLegend. Cells were then fixed by 15-min incubation in 2% paraformaldehyde on ice and analyzed on a BD LSRFortessa flow cytometer.

Statistical analysis

All data are presented as means \pm SEM, and statistical analyses were performed in Prism 8 (GraphPad Software Inc., La Jolla, CA). Statistical significance was defined as $P < 0.05$ following two-tailed t test, one-way analysis of variance (ANOVA), or two-way ANOVA as indicated within figure captions. Symbols denoting P values are as follows: * $P < 0.05$, ** $P < 0.01$, *** $P < 0.001$, and **** $P < 0.0001$.

Animal use

All animal procedures were performed at Georgia Institute of Technology and were approved by the Georgia Institute of Technology Institutional Animal Care and Use Committee. All mice were female C57BL6/J and were used at 10 to 18 weeks of age.

Supplementary Materials

This PDF file includes:

Figs. S1 to S10

[View/request a protocol for this paper from Bio-protocol.](#)

REFERENCES AND NOTES

- M. C. Mazzoni, T. C. Skalak, G. W. Schmid-Schönbein, Effects of skeletal muscle fiber deformation on lymphatic volumes. *Am. J. Physiol.* **259**, H1860–H1868 (1990).

2. T. C. Skalak, G. W. Schmid-Schönbein, B. W. Zweifach, New morphological evidence for a mechanism of lymph formation in skeletal muscle. *Microvasc. Res.* **28**, 95–112 (1984).
3. K. Nakamura, S. G. Rockson, The role of the lymphatic circulation in the natural history and expression of cardiovascular disease. *Int. J. Cardiol.* **129**, 309–317 (2008).
4. A. Aspelund, M. R. Robciuc, S. Karaman, T. Makinen, K. Alitalo, Lymphatic system in cardiovascular medicine. *Circ. Res.* **118**, 515–530 (2016).
5. L.-H. Huang, A. Elvington, G. J. Randolph, The role of the lymphatic system in cholesterol transport. *Front. Pharmacol.* **6**, 182 (2015).
6. C. Martel, W. Li, B. Fulp, A. M. Platt, E. L. Gautier, M. Westerterp, R. Bittman, A. R. Tall, S.-H. Chen, M. J. Thomas, D. Kreisler, M. A. Swartz, M. G. Sorci-Thomas, G. J. Randolph, Lymphatic vasculature mediates macrophage reverse cholesterol transport in mice. *J. Clin. Invest.* **123**, 1571–1579 (2013).
7. A. Milasan, F. Dallaire, G. Mayer, C. Martel, Effects of LDL receptor modulation on lymphatic function. *Sci. Rep.* **6**, 27862 (2016).
8. A. Taira, K. Uehara, S. Fukuda, K. Takenaka, M. Koga, Active drainage of cardiac lymph in relation to reduction in size of myocardial infarction: - An experimental study. *Angiology* **41**, 1029–1036 (1990).
9. K. S. Blum, S. Karaman, S. T. Proulx, A. M. Ochsenbein, P. Luciani, J.-C. Leroux, C. Wolfrum, M. Detmar, Chronic high-fat diet impairs collecting lymphatic vessel function in mice. *PLOS ONE* **9**, e94713 (2014).
10. E. S. Weitman, S. Z. Aschen, G. Farias-Eisner, N. Albano, D. A. Cuzzone, S. Ghanta, J. C. Zampell, D. Thorek, B. J. Mehrara, Obesity impairs lymphatic fluid transport and dendritic cell migration to lymph nodes. *PLOS ONE* **8**, e70703 (2013).
11. J. P. Scallan, M. A. Hill, M. J. Davis, Lymphatic vascular integrity is disrupted in type 2 diabetes due to impaired nitric oxide signalling. *Cardiovasc. Res.* **107**, 89–97 (2015).
12. S. Bilancini, M. Lucchi, S. Tucci, P. Eleuteri, Functional lymphatic alterations in patients suffering from lipedema. *Angiology* **46**, 333–339 (1995).
13. R. Tabibiazar, L. Cheung, J. Han, J. Swanson, A. Beilhack, A. An, S. S. Dadras, N. Rockson, S. Joshi, R. Wagner, S. G. Rockson, T. R. Cheung, H. J. Swanson, J. Beilhack, Inflammatory manifestations of experimental lymphatic insufficiency. *PLOS Med.* **3**, 254–1114 (2006).
14. O. Allam, K. E. Park, L. Chandler, M. A. Mozaffari, M. Ahmad, X. Lu, M. Alperovich, The impact of radiation on lymphedema: A review of the literature. *Gland Surg.* **9**, 596–602 (2020).
15. J. M. Armer, The problem of post-breast cancer lymphedema: Impact and measurement issues. *Cancer Invest.* **23**, 76–83 (2005).
16. T. B. Nutman, Insights into the pathogenesis of disease in human lymphatic filariasis. *Lymphat. Res. Biol.* **11**, 144–148 (2013).
17. C. L. Ly, R. P. Kataru, B. J. Mehrara, Inflammatory manifestations of lymphedema. *Int. J. Mol. Sci.* **18**, 171 (2017).
18. G. D. García Nores, C. L. Ly, I. L. Savetsky, R. P. Kataru, S. Ghanta, G. E. Hespse, S. G. Rockson, B. J. Mehrara, Regulatory T cells mediate local immunosuppression in lymphedema. *J. Invest. Dermatol.* **138**, 325–335 (2018).
19. S. H. Azhar, H. Y. Lim, B. K. Tan, V. Angeli, The unresolved pathophysiology of lymphedema. *Front. Physiol.* **11**, 137 (2020).
20. W. L. Olszewski, Contractility patterns of normal and pathologically changed human lymphatics. *Ann. N. Y. Acad. Sci.* **979**, 52–63 (2002).
21. S. Modi, A. W. B. Stanton, W. E. Svensson, A. M. Peters, P. S. Mortimer, J. R. Levick, Human lymphatic pumping measured in healthy and lymphoedematous arms by lymphatic congestion lymphoscintigraphy. *J. Physiol.* **583**, 271–285 (2007).
22. K. Nakamura, K. Radhakrishnan, Y. M. Wong, S. G. Rockson, Anti-inflammatory pharmacotherapy with ketoprofen ameliorates experimental lymphatic vascular insufficiency in mice. *PLOS ONE* **4**, e8380 (2009).
23. W. Tian, S. G. Rockson, X. Jiang, J. Kim, A. Begaye, E. M. Shuffle, A. B. Tu, M. Cribb, Z. Nepiyushchikh, A. H. Feroze, R. T. Zamanian, G. S. Dhillon, N. F. Voelkel, M. Peters-Golden, J. Kitajewski, J. B. Dixon, M. R. Nicolls, Leukotriene B4 antagonism ameliorates experimental lymphedema. *Sci. Transl. Med.* **9**, eaa13920 (2017).
24. N. Telinius, S. Mohanakumar, J. Majgaard, S. Kim, H. Pilegaard, E. Pahle, J. Nielsen, M. de Leval, C. Aalkjaer, V. Hjortdal, D. B. Boedtker, Human lymphatic vessel contractile activity is inhibited in vitro but not in vivo by the calcium channel blocker nifedipine. *J. Physiol.* **592**, 4697–4714 (2014).
25. K. H. T. To, P. Gui, M. Li, S. D. Zawieja, J. A. Castorena-Gonzalez, M. J. Davis, T-type, but not L-type, voltage-gated calcium channels are dispensable for lymphatic pacemaking and spontaneous contractions. *Sci. Rep.* **10**, 1–24 (2020).
26. H. M. Toland, K. D. McCloskey, K. D. Thornbury, N. G. Mchale, M. A. Hollywood, Ca²⁺-activated Cl⁻ current in sheep lymphatic smooth muscle. *Am. J. Physiol. Cell Physiol.* **279**, C1327–C1335 (2000).
27. S. D. Zawieja, J. A. Castorena-Gonzalez, J. P. Scallan, M. J. Davis, Differences in L-type Ca²⁺ channel activity partially underlie the regional dichotomy in pumping behavior by murine peripheral and visceral lymphatic vessels. *Am. J. Physiol. Hear. Circ. Physiol.* **314**, H991–H1010 (2018).
28. K. D. Cotton, M. A. Hollywood, N. G. Mchale, K. D. Thornbury, Outward currents in smooth muscle cells isolated from sheep mesenteric lymphatics. *J. Physiol.* **503**, 1–11 (1997).
29. N. A. Rohner, S. N. Thomas, Melanoma growth effects on molecular clearance from tumors and biodistribution into systemic tissues versus draining lymph nodes. *J. Control. Release* **223**, 99–108 (2016).
30. A. Schudel, L. F. Sestito, S. N. Thomas, Winner of the society for biomaterials young investigator award for the annual meeting of the society for biomaterials, April 11–14, 2018, Atlanta, GA: S-nitrosated poly(propylene sulfide) nanoparticles for enhanced nitric oxide delivery to lymphatic tissues. *J. Biomed. Mater. Res. Part A* **106**, 1463–1475 (2018).
31. I. Bodi, G. Mikala, S. E. Koch, S. A. Akhter, A. Schwartz, The L-type calcium channel in the heart: The beat goes on. *J. Clin. Invest.* **115**, 3306–3317 (2005).
32. D. Lipscombe, T. D. Helton, W. Xu, L-type calcium channels: The low down. *J. Neurophysiol.* **92**, 2633–2641 (2004).
33. J. Striessnig, A. Pinggera, G. Kaur, G. Bock, P. Tuluc, L-type Ca²⁺ channels in heart and brain. *Wiley Interdiscip. Rev. Membr. Transp. Signal.* **3**, 15–38 (2014).
34. G. T. Bolger, B. A. Weissman, P. Skolnick, The behavioral effects of the calcium agonist BAY K 8644 in the mouse: Antagonism by the calcium antagonist nifedipine. *Naunyn-Schmiedeberg's Arch. Pharmacol.* **328**, 373–377 (1985).
35. S. N. Thomas, E. Vokali, A. W. Lund, J. A. Hubbell, M. A. Swartz, Targeting the tumor-draining lymph node with adjuvanted nanoparticles reshapes the anti-tumor immune response. *Biomaterials* **35**, 814–824 (2014).
36. N. A. Rohner, S. N. Thomas, Flexible macromolecule versus rigid particle retention in the injected skin and accumulation in draining lymph nodes are differentially influenced by hydrodynamic size. *ACS Biomater. Sci. Eng.* **3**, 153–159 (2017).
37. N. L. Trevisan, L. M. Kaminskas, C. J. H. Porter, From sewer to saviour — Targeting the lymphatic system to promote drug exposure and activity. *Nat. Rev. Drug Discov.* **14**, 781–803 (2015).
38. M. An, M. Li, J. Xi, H. Liu, Silica nanoparticle as a lymph node targeting platform for vaccine delivery. *ACS Appl. Mater. Interfaces* **9**, 23466–23475 (2017).
39. A. Schudel, A. P. Chapman, M. Y. Kwan, C. J. Higgenson, D. M. Francis, M. P. Manspeaker, A. R. C. Avecilla, N. A. Rohner, M. G. Finn, S. N. Thomas, Programmable multistage drug delivery to lymph nodes. *Nat. Nanotechnol.* **15**, 491–499 (2020).
40. M. J. Weiler, M. T. Cribb, Z. Nepiyushchikh, T. S. Nelson, J. B. Dixon, A novel mouse tail lymphedema model for observing lymphatic pump failure during lymphedema development. *Sci. Rep.* **9**, 1–15 (2019).
41. M. P. Manspeaker, M. J. O. Melia, S. N. Thomas, Elicitation of stem-like CD8⁺ T cell responses via lymph node-targeted chemoimmunotherapy evokes systemic tumor control. *J. Immunother. Cancer* **10**, e005079 (2022).
42. M. S. Razavi, T. S. Nelson, Z. Nepiyushchikh, R. L. Gleason, J. B. Dixon, The relationship between lymphangion chain length and maximum pressure generation established through in vivo imaging and computational modeling. *Am. J. Physiol. Hear. Circ. Physiol.* **313**, H1249–H1260 (2017).
43. R. Moreau, F. Oberti, P. Lahaye, A. Gadano, S. Cailmail, P. Sogni, P. Cales, D. Lebrec, In vitro and in vivo vascular responses to the L-type calcium channel activator, Bay K 8644, in rats with cirrhosis. *J. Gastroenterol. Hepatol.* **13**, 1254–1258 (1998).
44. S. K. O'neill, G. T. Bolger, Enantiomer selectivity and the development of tolerance to the behavioral effects of the calcium channel activator BAY K 8644. *Brain Res. Bull.* **21**, 865–872 (1988).
45. A. Badou, M. K. Jha, D. Matza, R. A. Flavell, Emerging roles of L-type voltage-gated and other calcium channels in T lymphocytes. *Front. Immunol.* **4**, 243 (2013).
46. E. Shumilina, S. M. Huber, F. Lang, Ca²⁺ signaling in the regulation of dendritic cell functions. *Am. J. Physiol. Physiol.* **300**, C1205–C1214 (2011).
47. M. T. Cribb, L. F. Sestito, S. G. Rockson, M. R. Nicolls, S. N. Thomas, J. B. Dixon, The kinetics of lymphatic dysfunction and leukocyte expansion in the draining lymph node during LTb4 antagonism in a mouse model of lymphedema. *Int. J. Mol. Sci.* **22**, 4455 (2021).
48. N. Liu, B. Wang, Functional lymphatic collectors in breast cancer-related lymphedema arm. *Lymphat. Res. Biol.* **12**, 232–237 (2014).
49. K. Tashiro, J. Feng, S.-H. Wu, T. Mashiko, K. Kanayama, M. Narushima, H. Uda, S. Miyamoto, I. Koshima, K. Yoshimura, Pathological changes of adipose tissue in secondary lymphoedema. *Br. J. Dermatol.* **177**, 158–167 (2017).
50. J. M. Rutkowski, C. E. Markhus, C. C. Gyenge, K. Alitalo, H. Wiig, M. A. Swartz, Dermal collagen and lipid deposition correlate with tissue swelling and hydraulic conductivity in murine primary lymphedema. *Am. J. Pathol.* **176**, 1122–1129 (2010).
51. E. Gousopoulos, S. T. Proulx, J. Scholl, M. Uecker, M. Detmar, Prominent lymphatic vessel hyperplasia with progressive dysfunction and distinct immune cell infiltration in lymphedema. *Am. J. Pathol.* **186**, 2193–2203 (2016).
52. C. Zhou, W. Su, H. Han, N. Li, G. Ma, L. Cui, Mouse tail models of secondary lymphedema: Fibrosis gradually worsens and is irreversible. *Int. J. Clin. Exp. Pathol.* **13**, 54–64 (2020).

53. L. F. Sestito, S. N. Thomas, Biomaterials for modulating lymphatic function in immunoen지니어ing. *ACS Pharmacol. Transl. Sci.* **2**, 293–310 (2019).
54. M. G. Johnston, J. L. Gordon, Regulation of lymphatic contractility by arachidonate metabolites. *Nature* **293**, 294–297 (1981).
55. T. Ohhashi, R. Mizuno, F. Ikomi, Y. Kawai, Current topics of physiology and pharmacology in the lymphatic system. *Pharmacol. Ther.* **105**, 165–188 (2005).
56. J. J. Moon, H. Suh, A. V. Li, C. F. Ockenhouse, A. Yadava, D. J. Irvine, Enhancing humoral responses to a malaria antigen with nanoparticle vaccines that expand Tfh cells and promote germinal center induction. *Proc. Natl. Acad. Sci. U.S.A.* **109**, 1080–1085 (2012).
57. S. Kang, S. Ahn, J. Lee, J. Y. Kim, M. Choi, V. Gujrati, H. Kim, J. Kim, E. C. Shin, S. Jon, Effects of gold nanoparticle-based vaccine size on lymph node delivery and cytotoxic T-lymphocyte responses. *J. Control. Release* **256**, 56–67 (2017).
58. L. F. Sestito, S. N. Thomas, Lymph-directed nitric oxide increases immune cell access to lymph-borne nanoscale solutes. *Biomaterials* **265**, 120411 (2020).
59. C. Hadamitzky, R. Pabst, Acquired lymphedema: An urgent need for adequate animal models. *Cancer Res.* **68**, 343–345 (2008).
60. W. S. Shin, A. Szuba, S. G. Rockson, Animal models for the study of lymphatic insufficiency. *Lymphat. Res. Biol.* **1**, 159–169 (2003).
61. J. M. Rutkowski, M. Moya, J. Johannes, J. Goldman, M. A. Swartz, Secondary lymphedema in the mouse tail: Lymphatic hyperplasia, VEGF-C upregulation, and the protective role of MMP-9. *Microvasc. Res.* **72**, 161–171 (2006).
62. Y. Yoon, T. Murayama, E. Gravereaux, T. Tkebuchava, M. Silver, C. Curry, A. Wecker, R. Kirchmair, C. S. Hu, M. Kearney, A. Ashare, D. G. Jackson, H. Kubo, J. M. Isner, D. W. Losordo, VEGF-C gene therapy augments postnatal lymphangiogenesis and ameliorates secondary lymphedema. *J. Clin. Invest.* **111**, 717–725 (2003).
63. G. D. García Nores, C. L. Ly, D. A. Cuzzone, R. P. Kataru, G. E. Hespe, J. S. Torrisi, J. J. Huang, J. C. Gardenier, I. L. Savetsky, M. D. Nitti, J. Z. Yu, S. Rehal, B. J. Mehrara, CD4⁺ T cells are activated in regional lymph nodes and migrate to skin to initiate lymphedema. *Nat. Commun.* **9**, 1970 (2018).
64. S. Ghanta, D. A. Cuzzone, J. S. Torrisi, N. J. Albano, W. J. Joseph, I. L. Savetsky, J. C. Gardenier, D. Chang, J. C. Zampell, B. J. Mehrara, Regulation of inflammation and fibrosis by macrophages in lymphedema. *Am. J. Physiol. Hear. Circ. Physiol.* **308**, H1065–H1077 (2015).
65. A. Rehor, J. A. Hubbell, N. Tirelli, Oxidation-sensitive polymeric nanoparticles. *Langmuir* **21**, 411–417 (2005).
66. M. J. Davis, J. P. Scallan, J. H. Wolpers, M. Muthuchamy, A. A. Gashev, D. C. Zawieja, Intrinsic increase in lymphangion muscle contractility in response to elevated afterload. *Am. J. Physiol. Hear. Circ. Physiol.* **303**, H795–H808 (2012).
67. J. A. Kornuta, J. B. Dixon, Ex vivo lymphatic perfusion system for independently controlling pressure gradient and transmural pressure in isolated vessels. *Ann. Biomed. Eng.* **42**, 1691–1704 (2014).
68. J. A. Kornuta, Z. Nepiyushchikh, O. Y. Gasheva, A. Mukherjee, D. C. Zawieja, J. B. Dixon, Effects of dynamic shear and transmural pressure on wall shear stress sensitivity in collecting lymphatic vessels. *Am. J. Physiol. Regul. Integr. Comp. Physiol.* **309**, R1122–R1134 (2015).
69. A. A. Gashev, M. J. Davis, M. D. Delp, D. C. Zawieja, Regional variations of contractile activity in isolated rat lymphatics. *Microcirculation* **11**, 477–492 (2004).
70. M. Weiler, T. Kassis, J. B. Dixon, Sensitivity analysis of near-infrared functional lymphatic imaging. *J. Biomed. Opt.* **17**, 066019 (2012).
71. M. Weiler, J. B. Dixon, Differential transport function of lymphatic vessels in the rat tail model and the long-term effects of Indocyanine Green as assessed with near-infrared imaging. *Front. Physiol.* **4**, 215 (2013).

Acknowledgments: We thank K. Binz for technical assistance. **Funding:** This work was supported by U.S. National Institutes of Health grants R01HL133216 (to J.B.D.), R01CA207619 (to S.N.T.), R01CA247484 (to S.N.T.), U01CA214354 (to S.N.T.), and T32EB006343 (to L.F.S.); American Heart Association grant 19PRE34430140 (to L.F.S.); and the Lipedema Foundation (to K.H.T.T.). **Author contributions:** Conceptualization: L.F.S., K.H.T.T., S.N.T., and J.B.D. Methodology: L.F.S., K.H.T.T., S.N.T., and J.B.D. Formal analysis: L.F.S., K.H.T.T., M.T.C., and P.A.A. Investigation: L.F.S., K.H.T.T., and M.T.C. Writing (original draft): L.F.S. Writing (review and editing): L.F.S., K.H.T.T., M.T.C., P.A.A., S.N.T., and J.B.D. Visualization: L.F.S., K.H.T.T., M.T.C., and P.A.A. Supervision: S.N.T. and J.B.D. Project administration: S.N.T. and J.B.D. Funding acquisition: S.N.T. and J.B.D. **Competing interests:** The authors declare that they have no competing interests. **Data and materials availability:** All data needed to evaluate the conclusions in the paper are present in the paper and/or the Supplementary Materials.

Submitted 15 March 2022

Accepted 20 January 2023

Published 24 February 2023

10.1126/sciadv.abq0435